

Optical Microsensor for Continuous Glucose Measurements in Interstitial Fluid

Jonathon T. Olesberg,^{a,d} Chuanshun Cao,^{b,d} Jeffrey R. Yager,^{b,d} John P. Prineas,^{b,d}
Chris Coretsopoulos,^{b,c,d} Mark A. Arnold,^{a,c} Linda J. Olafsen,^e and Michael Santilli^e

^aDepartment of Chemistry, University of Iowa, Iowa City, IA

^bDepartment of Physics, University of Iowa, Iowa City, IA

^cDepartment of Chemical Engineering, University of Iowa, Iowa City, IA

^dOptical Science and Technology Center, University of Iowa, Iowa City, IA

^eDepartment of Physics and Astronomy, University of Kansas, Lawrence, KS

ABSTRACT

Tight control of blood glucose levels has been shown to dramatically reduce the long-term complications of diabetes. Current invasive technology for monitoring glucose levels is effective but underutilized by people with diabetes because of the pain of repeated finger-sticks, the inconvenience of handling samples of blood, and the cost of reagent strips. A continuous glucose sensor coupled with an insulin delivery system could provide closed-loop glucose control without the need for discrete sampling or user intervention. We describe an optical glucose microsensor based on absorption spectroscopy in interstitial fluid that can potentially be implanted to provide continuous glucose readings. Light from a GaInAsSb LED in the 2.2–2.4 μm wavelength range is passed through a sample of interstitial fluid and a linear variable filter before being detected by an uncooled, 32-element GaInAsSb detector array. Spectral resolution is provided by the linear variable filter, which has a 10 nm band pass and a center wavelength that varies from 2.18–2.38 μm ($4600\text{--}4200\text{ cm}^{-1}$) over the length of the detector array. The sensor assembly is a monolithic design requiring no coupling optics. In the present system, the LED running with 100 mA of drive current delivers 20 nW of power to each of the detector pixels, which have a noise-equivalent-power of 3 pW/Hz^{1/2}. This is sufficient to provide a signal-to-noise ratio of 4500 Hz^{1/2} under detector-noise limited conditions. This signal-to-noise ratio corresponds to a spectral noise level less than 10 μAU for a five minute integration, which should be sufficient for sub-millimolar glucose detection.

Keywords: glucose, diabetes, non-invasive, LED, detector array, microsensor, linear variable filter

1. INTRODUCTION

Diabetes is a chronic, incurable disease that causes an array of serious medical complications and premature death. Complications of diabetes include heart disease, stroke, kidney failure, blindness, amputations and nervous system disorders. The Centers for Disease Control and Prevention reports that each year an estimated 12,000 to 24,000 people with diabetes become blind, more than 43,000 begin treatment for kidney failure, and 82,000 require amputations. In addition to pain and suffering, these complications are costly.¹ The American Diabetes Association estimates that the total cost of diabetes in the United States was \$98 billion dollars in 1997. This amount corresponds to both direct healthcare costs (\$44 billion) and the indirect costs (\$54 billion) associated with disability, premature mortality and loss of work.^{2,3}

The prevalence of diabetes is growing at an alarming rate both in the U.S. and internationally. A recent report from the Centers for Disease Control and Prevention shows that the incidence of diabetes in the United States increased by 33% from 1990 to 1998. More startling is their estimate that over this period the incidence of diabetes increased by 70% for people in their 30s.⁴ The World Health Organization warns of a diabetes epidemic on the basis of a tremendous increase in the incidence of diabetes worldwide. Their figures indicate that the number of people with diabetes increased from 30 million in 1985 to 135 million in 1999, and they project that 300 million people will have diabetes by 2025.⁵ Although diabetes is a potentially devastating disease, early diagnosis

Further author information: (email) jonathon-olesberg@uiowa.edu, (email) mark-arnold@uiowa.edu

and tight glycemic control can greatly diminish the medical complications and cost of this disease. The goal of tight control is to maintain one's blood glucose levels within a physiologically acceptable range. Tight control requires frequent blood glucose measurements, which provides the information needed to administer insulin or glucose properly in order to avoid chronic hyperglycemia and acute hypoglycemia. The benefits of tight control are well-documented⁶⁻⁸ and stem from a delay in the onset of the medical complications created by chronic hyperglycemia. Unfortunately, early diagnosis and tight glycemic control are not adequately achieved. The NIH reports that of the 15.7 million Americans with diabetes, 5.4 million people remain undiagnosed (34%). In addition, recent studies indicate that a vast majority of Americans with type I diabetes only measure their blood glucose levels once per day, which is insufficient to maintain tight control.³ The pain, cost and inconvenience of even state-of-the-art glucose monitoring technology impede frequent monitoring and are primarily responsible for the failure of patients to maintain tight control.

It has been recognized for several decades that the ideal treatment of diabetes would involve a closed-loop insulin delivery system that is implanted within the patient's body. The so-called artificial pancreas consists of an insulin delivery pump coupled with some type of glucose-sensing technology. Insulin is delivered continuously in response to detected changes in the blood glucose concentrations. For this to work, the glucose sensing component must be able to provide accurate and rapid blood glucose values to a micro-processing unit, which computes the amount of insulin required and then controls insulin delivery. The key limitation to the successful development of an artificial pancreas is the implantable glucose sensing technology.

The eventual objective of this research program is to develop the technology for an implantable glucose sensor that provides continuous and reagent-free optical analysis of interstitial fluid (ISF). During operation, the ISF is sampled through an embedded microprobe and enters into a microfluidic chamber, which guides the ISF sample through a miniaturized spectrometer. A near-infrared spectrum is collected and the concentration of glucose is obtained from direct analysis of this spectrum.

The concept of measuring glucose in ISF and the relation of this value to the more clinically acceptable blood glucose concentration has been established by others. Many research groups report correlations between glucose concentrations in ISF and blood.⁹⁻¹³ In all cases, a clinically significant correlation is noted, although the dynamics of this correlation are the subject of continued examination.¹⁴

The concept of drawing ISF by either microdialysis or ultrafiltration has been reported previously.¹⁵⁻¹⁹ Microdialysis, in particular, has been used to examine the correlation between the concentrations of glucose in blood and ISF. For example, Janle and Kissinger successfully sampled ISF from rats by ultrafiltration and found that the levels of glucose in the sampled ISF fluids correlate strongly to levels in blood.²⁰ In addition, Janle and Kissinger found that the ISF could be sampled over many days without significant degradation in the sampling properties of the probe.

Crucial to the success of this integrated sensor is the development of a mechanism to sample glucose subcutaneously in a continuous fashion. Previous studies involving humans have relied upon either ultrafiltration^{21, 22} or microdialysis sampling^{23, 24} to accomplish this task. Both microdialysis sampling and ultrafiltration employ semi-permeable membranes that are implanted in the tissue of interest and allow studies to be conducted in awake moving animals or human subjects.²⁵

Previous work has shown that both ultrafiltration and microdialysis can effectively sample ISF in humans for weeks to a month.²¹⁻²³ Both are separation techniques that involve moving the analyte across a semi-permeable membrane. Because of the hydrophobicity and molecular weight cutoff of the membrane, the techniques are well-suited to sample hydrophilic substances and result in sampled solutions that are free of proteins, cells, and enzymes.²⁶ A major issue that arises when using microdialysis sampling is the exact determination of the analyte recovery.^{22, 26} To circumvent this problem, ultra-slow microdialysis has been successfully used to ensure close to 100% recovery for glucose in ISF.^{23, 24, 27} Since ISF is rapidly replenished and the amount of fluid that is removed is small with respect to the entire pool, the continued removal of ISF does not pose a problem in subcutaneous sampling.^{20, 25} In ultrafiltration, because there is bulk flow across the membrane and there is no perfusate to dilute the collected analyte, relative recoveries for glucose are generally around 100% and are not affected by fibrous layers that may form around the probe.^{20, 25} However, the flow rate is dependent upon the surface area of the probe and fibrin formation around the probe.²⁰

Ash *et al.* used ultrafiltration to sample ISF continually from human diabetic patients.²¹ Ultrafiltration probes were implanted subcutaneously in the mid-abdomen. No sutures were required and there was no reported post-operative bleeding or tenderness.²¹ An evacuated vial (vacutainer) was used to supply the vacuum to pull the ISF through the membrane. The ultrafiltration probes were left in place and sampled continuously for one month. Steady flow rates of 40–60 $\mu\text{l/hr}$ were achieved by use of vacutainers over the one-month period. The amount of glucose in the ISF was measured off-line by an electrochemical glucose oxidase method and a correlation between blood and ISF glucose concentrations was observed.²¹ Baumeister and co-workers later utilized ultra-slow microdialysis sampling to monitor glucose in the ISF of neonates.²³ The microdialysis probes were implanted subcutaneously in the lateral thigh and sampled continuously for up to 16 days. A perfusate flow rate of 300 nL/min was used and near unitary recovery was achieved (96%). The amount of glucose in the ISF was measured off-line by an enzyme spectrophotometric method and again, a correlation between the blood and ISF glucose concentrations was seen.²³ Rhemrev-Boom *et al.* have also utilized ultraslow microdialysis to perform a similar measurement.²⁴ A lightweight measuring device consisting of a vacuum chamber (monovette) and a portable potentiostat were used to measure glucose continuously with an enzyme/electrochemical method.²⁴ The potential for a portable method to monitor glucose remotely in ISF was shown, although the instability of the biosensor portion of the device limited the lifetime of the device to three days.

These studies show that long-term (weeks to a month) sampling of ISF in humans is possible by both ultrafiltration and microdialysis and each technique gives a good correlation to the concentration of glucose in blood. These findings also demonstrate the possibility of remote, unattended monitoring.

2. DESIGN AND RESULTS

Our immediate goal is to develop an optical microsensor that can be used in conjunction with ultrafiltration or microdialysis for continuous monitoring of interstitial fluid glucose levels. One of the constraints in this strategy is that the sensor be able to run off a battery for at least 24 hrs between recharging. This limits the total current that the sensor can draw and precludes the use of thermoelectrically cooled detectors. In addition, the system must be as small as possible and rugged enough to operate within the body for up to a year.

The core of the integrated near-IR sensor consists of four components: a broadband LED light source, an optical sampling chamber, a linearly variable optical filter, and an array of photodetector elements. The arrangement of these components is shown in Fig. 1. Fluid will enter and exit the optical sampling chamber by way of microbore tubing. Light will pass from the LED through the sampling chamber, through the spatially variable filter, and be detected by the photodiode array. The optical sensor contains no moving or adjustable parts and can in principle occupy as little as a one tenth of a cubic centimeter of volume.

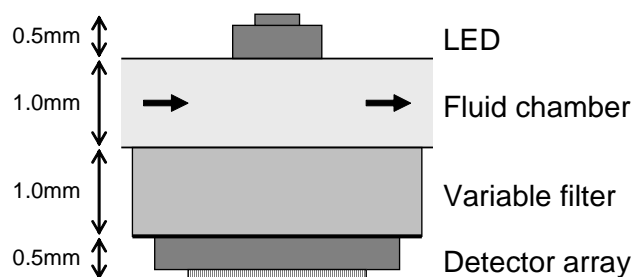


Figure 1. Schematic of the key components in the near-infrared microsensor. The LED is bonded to the fluid chamber substrate-side down which leaves the electrical contacts exposed from the top. The linear variable filter is bonded to the opposite side of the flow system with the coating facing down. The substrate side of the detector array is then bonded to the variable filter with the electrical contacts exposed to the bottom. The thickness of each of the components is indicated. The figure is to scale.

2.1. Optical Source

A GaInAsSb LED is used as the optical source for the system. The GaInAsSb material system has a cutoff wavelength that can be varied from 1.5–4.1 μm while maintaining lattice match to a GaSb substrate. The materials used in this work were grown by molecular beam epitaxy on GaSb substrates. The band gap of the light-emitting region has been tailored to match the key glucose features in the combination band. The most significant spectral features for glucose are the two C-H features at 4300 and 4400 cm^{-1} , which are covered by the emission of the LED. Wavelength optimization, which is performed as a standard step in PLS model calibration, normally isolates this region when using high-quality spectra (i.e., calibration models perform better without spectral information from outside this range). The broad O-H feature at 4700 cm^{-1} is too broad to provide useful chemical information. The spectral width for LED emission is typically $2k_B T$, where k_B is Boltzmann's constant and T is the temperature in Kelvin. For body temperature operation, this is equivalent to 400 cm^{-1} (200 nm). By selecting a band gap of 4200 cm^{-1} (2.38 μm), we cover the key glucose-specific features in the combination region of the near infrared spectrum.

The LED is based on a simple *p-i-n* heterojunction with GaSb as the barrier material.²⁸ The principal design issue for the LED is the internal quantum efficiency, which is the relative probability of radiative versus nonradiative recombination processes. The dominant nonradiative recombination process at low carrier concentrations is Shockley-Read-Hall recombination, with a typical carrier lifetime for high-quality material of 10 ns. As the carrier concentration is increased, the probability of radiative recombination increases, as does the Auger recombination rate. At sufficiently high carrier densities Auger recombination will dominate. There is thus an intermediate density when the ratio of radiative to nonradiative recombination is the highest. Given typical radiative and Auger recombination rates in this material system we estimate the optimal carrier density to be $2 \times 10^{17} \text{ cm}^{-3}$, corresponding to an internal radiative efficiency of 4%.

Although LEDs are very efficient emitters as compared with Globars or tungsten lamps, the LED will have the largest power draw of any component in the system. This means that the efficiency of the LED will dominate the operation time available from a single battery. Unfortunately, both the LED drive voltage (0.6 V) and current (~ 500 mA) are mismatched with typical battery sources as well as the rest of the electronics (3.3 V and 10 mA). Both of these mismatches can be addressed by utilizing active region cascading. A conventional LED incorporates a single emitting layer in the center of a *p-i-n* diode junction. In a cascaded system, several *p-i-n* junctions are cascaded in series using Esaki tunnel junctions. Using a cascade of 5 emitter regions will increase the voltage requirement and decrease the current draw by a factor of 5 (to 3.0 V and 100 mA) without changing the output optical power. This modification should significantly extend battery life, which will be especially critical for an eventual implanted sensor.

The LED's are fabricated using a back-side emitting geometry, so the light generated in the active volume of the LED exits the device through the substrate opposite the electrical contacts. This allows the LED to be bonded directly to the fluid flow chamber with the electrical contacts still accessible. The direct coupling of the LED to the chamber with no air gap also provides an efficient immersion coupling. The LED is mounted contact-side down on a header to facilitate handling and electrical connection.

An emission spectrum from one of the five-stage LED's is shown in Fig. 2 along with the absorptivity spectrum of glucose. The LED emission covers the three primary glucose absorption features within the combination band. If necessary, the emission spectrum can be broadened and flattened by grading the wavelength of each of the cascaded emitters. The on-axis output power of the LED is 150 $\mu\text{W}/\text{sr}$ at 100 mA.

2.2. Fluid Chamber

The fluid chamber must be capable of providing an optical path length of approximately 1 mm in order to maximize the signal-to-noise-ratio.²⁹ Given the limited flow rates associated with interstitial fluid collection, it is important to minimize the optical chamber's volume. In our system, a 1 cm long, square, thin-walled capillary with a 0.8 mm inner dimension is used. Fluid is delivered to and extracted from the capillary with microbore Tygon tubing with an inner diameter of 0.010 in.

The volume of the optical chamber is 6 μl . The total volume of the 30 cm long flow system before and including the optical cell is less than 30 μl . For an interstitial collection rate of 50 $\mu\text{l}/\text{min}$, the transit time from the ultrafiltration membrane to the end of the flow chamber will be 36 sec.

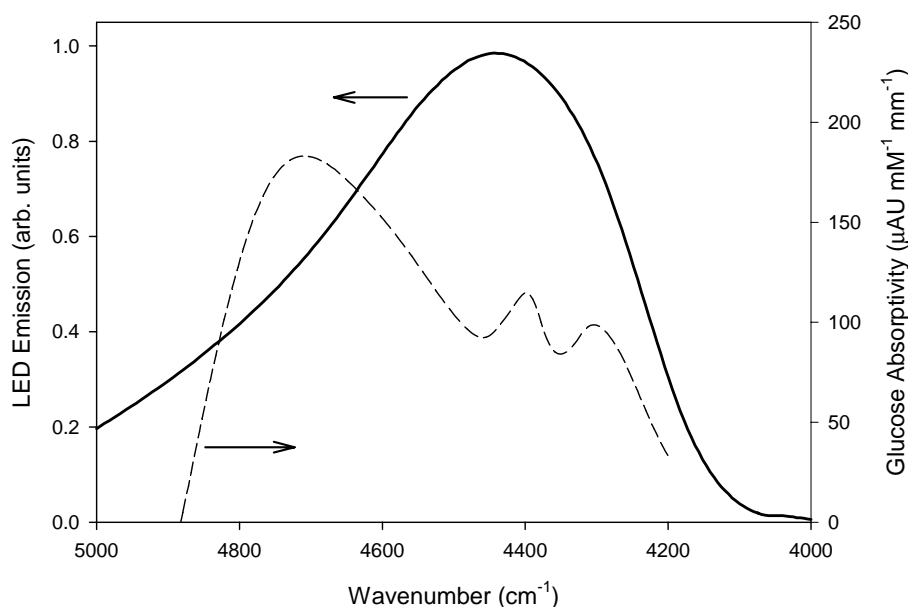


Figure 2. Left axis: LED emission spectrum (solid) of a five-stage device operating at 100 mA. Right axis: Glucose absorptivity spectrum (dashed). The LED emission spans the critical absorption features of glucose at 4300, 4400, and 4700 cm^{-1} .

Vacuum to draw the interstitial fluid through the ultrafiltration probe and the optical chamber will initially be provided by a syringe pump for *in vitro* work and a vacutainer for *in vivo* studies. Eventually, a microfluidic or miniaturized pump could be integrated with the system to provide continuous flow.

2.3. Spectrometer

There are several strategies for performing spectrally resolved measurements, including Fourier transform and dispersive techniques (utilizing a diffraction grating or other dispersive element). The system presented here employs an alternative strategy that is simple, rugged, and compact. Light exiting the fluid chamber is incident on a linearly variable bandpass filter, which is mounted directly on top of a linear photodiode array. The filter is designed such that the central wavelength of the passband varies along one of the dimensions of the filter. Thus, each detector element is sensitive to a different wavelength. The spectral resolution is determined by the width of the passband at each point, and the spectral point spacing is determined by the number of detector array elements. Unlike diffraction-based instruments, this strategy requires no imaging optics. The filter and detector assembly can be mounted directly on the output of the fluid chamber. The linearly variable filter was purchased from Optical Coating Laboratory, Inc., which specializes in variable filters for this type of spectroscopy. The filter has a passband width of 20 cm^{-1} , which we have previously demonstrated to be adequate for measurement of glucose in aqueous solutions.³⁰

An array of unbiased GaInAsSb *p-i-n* diodes is used for the photodetectors. The light-absorbing *i* layer consists of $2.5 \mu\text{m}$ of the GaInAsSb alloy. The target band gap for the detector is approximately 4000 cm^{-1} ($2.5 \mu\text{m}$), which is slightly longer wavelength than used for the LED so that the absorption coefficient in the target wavelength range will be large (5000 cm^{-1}) at the wavelength of the glucose absorption features. The absorption length for 4300 cm^{-1} light in the GaInAsSb alloy is $2 \mu\text{m}$, so that the majority of the light will be absorbed in an *i* layer. Electron diffusion lengths in these materials also influence the choice of *i* layer thickness. Typical mobilities are $3000 \text{ cm}^2/\text{Vs}$ at room temperature, and typical minority electron lifetimes in very high-quality undoped materials are 10 ns, so carriers can diffuse across an *i* layer $10 \mu\text{m}$ thick. Even accounting for a minority

carrier lifetime of 3 ns, the $2.5\ \mu\text{m}$ i thickness should not pose a problem for carrier diffusion. By ensuring that as many created electron-hole pairs are collected as possible, this approach maximizes the responsivity.

Detector noise is the key limitation to high-quality spectral measurements in the near-IR combination region. To minimize detector noise, conventional spectrometer systems utilize liquid nitrogen or multi-stage thermoelectric cooling of the detector element. However, neither of these is practical for a portable, battery-operated device (typical thermoelectric cooling requirements are 2–5 W). To be practical, a battery-operated, potentially implantable sensor must be able to operate successfully with an uncooled (ambient or body-temperature) detector. The noise produced by a detector element is proportional to the square root of its area. Thus, one way to reduce the impact of detector noise is to minimize the size of the detector, provided that the amount of light collected is held constant. For conventional instruments, the use of a low-brightness, broadband source (such as a tungsten lamp) means that small detector elements are not advantageous. However, because we will be using a high-brightness LED only 3 mm from the detector, we can use very small detector elements in order to minimize detector noise. (Note that “high-brightness” refers to the optical power emitted in the wavelength range of interest relative to the emission area. By this definition, the proposed LED is significantly “brighter” than a tungsten lamp or Globar source, even though the latter produce significantly more total optical power).

Like the LED, the detector array is fabricated using a back-side geometry, meaning that light enters the device through the side opposite that of the contacts. A photograph of a fabricated detector array is shown in Fig. 3. The metal pads on the left and right edges are the common cathode contacts. Each of the vertical bars in the center is the anode contact of an independent detector mesa. Each pixel is $50\ \mu\text{m}$ in width and 1 mm long. The space between pixels is $10\ \mu\text{m}$. The square bonding pads at the end of each bar are $100\ \mu\text{m}$ on a side.

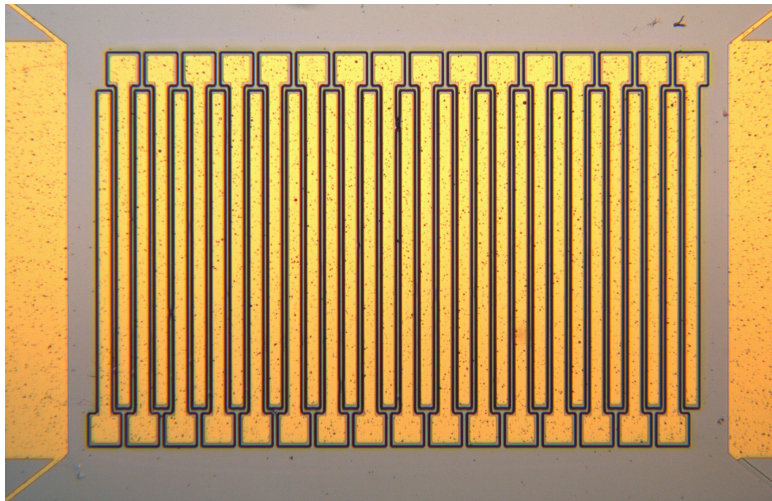


Figure 3. Photographs of a completed detector array. The vertical bars are independent pixel mesas that are $50\ \mu\text{m}$ wide and 1 mm long separated by $10\ \mu\text{m}$ gaps. The squares at the top and bottom are $100\ \mu\text{m}$ contact pads. Light enters the device from the back side, so the entire pixel surface can be metallized.

The detector pixels of first-generation devices have a zero-bias resistance greater than $3\ \text{k}\Omega$ and a peak responsivity of $0.8\ \text{A/W}$. This implies a 300K specific detectivity of $0.8 \times 10^{10}\ \text{cm Hz}^{1/2}\ \text{W}^{-1}$ and a noise-equivalent power of $3.0\ \text{pW/Hz}^{1/2}$. Detector materials with larger resistivity have recently been obtained through controlled doping of the absorber region and should reduce the noise-equivalent power of the pixels.

The detector arrays are bonded contact-side down onto a header with contacts matching the pixel bonding pads. This header is then mounted in a 40-pin DIP package chip-carrier to simplify handling during the prototype phase. The linear variable filter is bonded on top of the detector array. A photograph of the completed spectrometer portion of the microsensors is shown in Fig. 4.

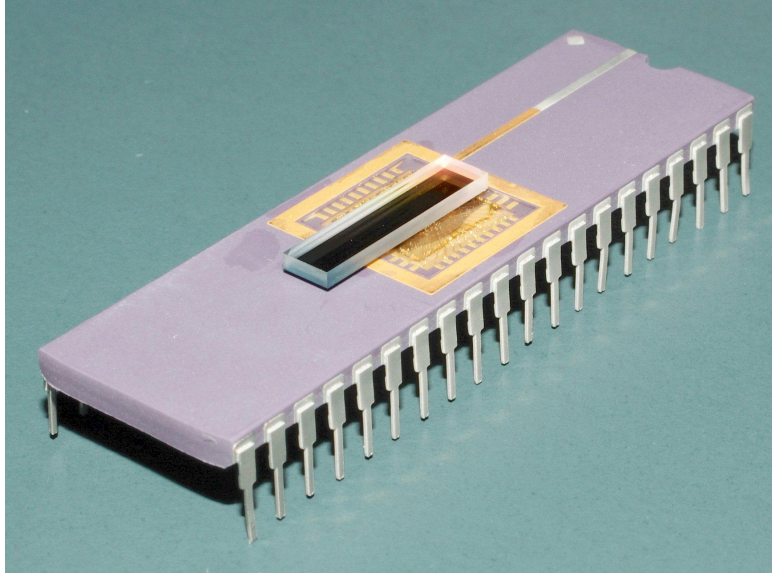


Figure 4. Linear variable filter and detector array subassembly on a 40-pin DIP chip carrier.

The normalized response of each of the array pixels was measured with a Fourier transform spectrometer and is shown in Fig. 5. The pixels have an average full-width at half maximum of 28 cm^{-1} (14 nm). There is some distortion visible in the $4250\text{--}4300\text{ cm}^{-1}$ range that is likely due to electrical shorting between pixels. The absolute response of the majority of the pixels lies within a $\pm 10\%$ window.

2.4. Sensor Assembly

The LED and spectrometer subassemblies are bonded directly onto opposite sides of the fluid chamber. The assembly as a whole can be encapsulated in order to improve its structural strength. A photograph of the assembled system is shown in Fig. 6. The package can be installed in a 40-pin socket to provide connection to the read-out electronics. In the future, the chip carrier can be eliminated and the unit integrated directly with the read-out and LED drive circuits. The microsensor is shown from the side in Fig. 7. The optical components are indicated with arrows. The core of the microsensor is highlighted with the dashed line and occupies only 0.03 cm^3 .

The noise characteristics of the unit have been measured using a nominal LED current of 100 mA modulated by a 50% duty cycle square wave. At this drive level, the measured spectral noise on back-to-back water spectra is $16\text{ }\mu\text{AU}$ for a 60 s average or $7\text{ }\mu\text{AU}$ for a 5-minute average. This value is close to the $5\text{ }\mu\text{AU}$ value predicted based on detector-noise limited operation.

3. CONCLUSIONS

We report the initial development of an optical microsensor for the measurement of glucose in interstitial fluid. The system is capable of measuring the transmission spectrum of a $6\text{ }\mu\text{l}$ sample with a spectral resolution of 28 cm^{-1} in the $4200\text{--}4600\text{ cm}^{-1}$ range. The present system provides a spectral noise level of $16\text{ }\mu\text{AU}$ for a 60 s integration.

There are two primary avenues for improving the performance of the current system. The first will be to increase the specific detectivity of the detector elements. This is being pursued by working to improve the fundamental quality of the materials grown by molecular beam epitaxy and through improvements in processing methods, such as the use of surface passivation to reduce leakage current. It is expected that an increase in detectivity of up to one order of magnitude can be obtained. The second avenue is to increase the optical collection and delivery of light through the system. This can be obtained by thinning components such as the

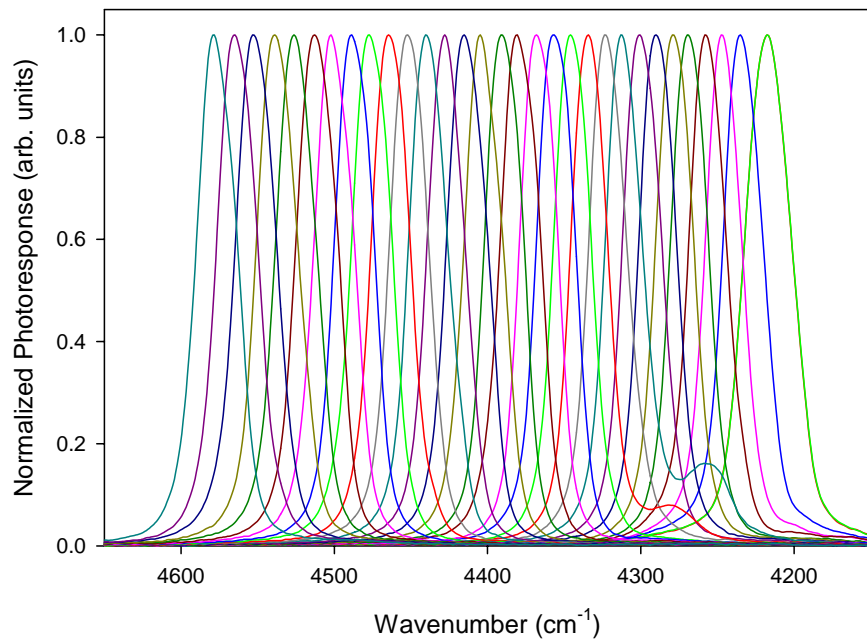


Figure 5. Normalized spectral response of each pixel in the array measured with a Fourier Transform spectrometer. The average full-width at half maximum is 28 cm^{-1} . There is a shoulder on the response of two of the pixel responses between 4250 and 4300 cm^{-1} that is likely due to shorting between pixels.

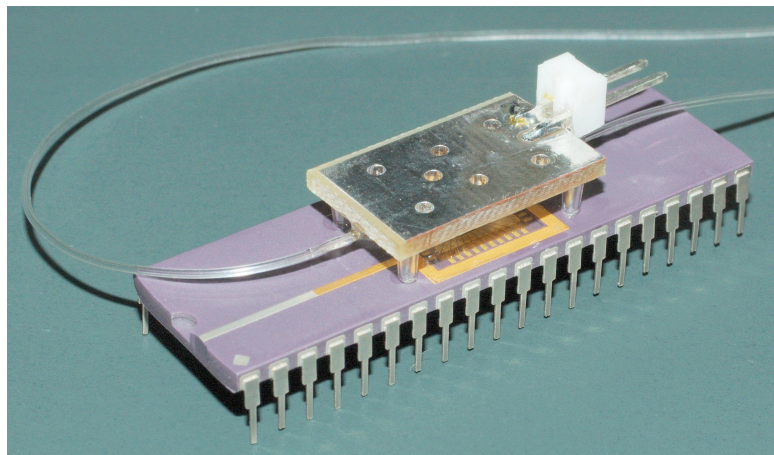


Figure 6. Assembled microsensor.

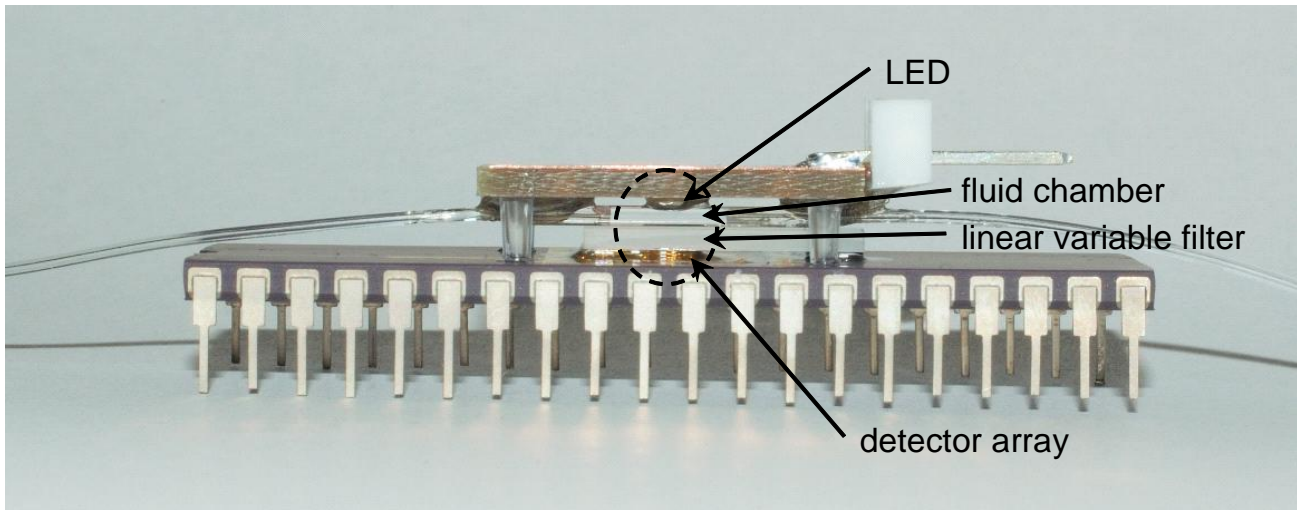


Figure 7. Assembled microsensor viewed from the side. The active components (highlighted by the dashed oval) occupy a fraction of the total volume. These components can in principle be packaged into a much smaller volume for implantation.

linear variable filter so as to increase the collection solid angle. Also, it may be possible to plate the inner sides of the capillary with a reflective material in order to guide the light through the chamber. Improvements in system performance level can be used to improve the accuracy of the measurement, provide more frequent predictions, or allow powering-off the system to extend battery life.

ACKNOWLEDGMENTS

This research was supported by grants from the National Institute of Diabetes and Digestive and Kidney Diseases of the National Institutes of Health (DK-64569 and DK-02925).

REFERENCES

1. U.S. Department of Health and Human Services, Centers for Disease Control and Prevention, "The burden of chronic diseases and their risk factors: national and state perspectives," February 2004. http://www.cdc.gov/nccdphp/burdenbook2004/pdf/burden_book2004.pdf.
2. American Diabetes Association, "Economic consequences of diabetes mellitus in the U.S. in 1997," *Diabetes Care* **21**, pp. 296–309, 1998.
3. *Diabetes in America*, Publication No. 95-1468, National Diabetes Data Group, National Institutes of Health, National Institute of Diabetes and Digestive and Kidney Diseases, 2nd ed., 1995.
4. A. H. Mokdad, E. S. Ford, B. A. Bowman, D. E. Nelson, M. M. Engelgau, F. Vinicor, and J. S. Marks, "Diabetes trends in the U.S.," *Diabetes Care* **23**, pp. 1278–1283, 2000.
5. "World Health Organization fact sheet, no. 236," September 1998. <http://www.who.int/mediacentre/factsheets/fs236/en/>.
6. Diabetes Control and Complications Trial Research Group, "The effect of intensive treatment of diabetes on the development and progression of long-term complications in insulin-dependent diabetes mellitus," *N Engl J Med* **329**, pp. 977–986, September 1993.
7. UK Prospective Diabetes Study Group, "Intensive blood-glucose control and sulphonylureas or insulin compared with conventional treatment and risk of complications in patients with type 2 diabetes," *Lancet* **352**, pp. 837–853, 1998.
8. Y. Ohkubo, "Intensive insulin therapy prevents the progression of diabetic microvascular complications in Japanese patients with non-insulin-dependent diabetes mellitus: A randomized prospective 6-year study," *Res Clin Pract* **28**, pp. 103–117, 1995.

9. M. E. Collison and P. J. Stout, "Analytical characterization of electrochemical biosensor test strips for measurement of glucose in low-volume interstitial fluid samples," *Clin Chem* **45**, pp. 1665–1673, 1999.
10. J. A. Tamada, S. Garg, L. Jovanovic, K. R. Pitzer, S. Fermi, and P. R. O, "Noninvasive glucose monitoring: Comprehensive clinical results," *J Am Med Assoc* **282**, pp. 1839–1844, 1999.
11. F. Sternberg, C. Meyerhoff, F. Mennel, H. Mayer, F. Bischof, and E. Pfeiffer, "Does fall in tissue glucose precede fall in blood glucose?," *Diabetologia* **39**, pp. 609–612, 1996.
12. C. Meyerhoff, F. Bischof, F. Sternberg, H. Zier, and E. Pfeiffer, "On line continuous monitoring of subcutaneous tissue glucose in men by combining portable glucosensor with microdialysis," *Diabetologia* **35**, pp. 1087–1092, 1992.
13. V. Thome-Duret, G. Reach, M. Gangnerau, F. Lemonnier, J. Klein, Y. Zhang, Y. Hu, and G. Wilson, "Use of subcutaneous glucose sensor to detect decreases in glucose concentration prior to observation in blood," *Anal Chem* **68**, pp. 3822–3826, 1996.
14. D. W. Schmidtke, A. C. Freeland, A. Heller, and B. R. T., "Measurement and modeling of the transient difference between blood and subcutaneous glucose concentrations in a rat after injection of insulin," *Proc Natl Acad Sci USA* **95**, pp. 294–299, 1998.
15. W. Kerner, "Implantable glucose sensors: present status and future developments," *Exper Clin Endocrinol Diabetes* **2**, pp. S341–S346, 2001.
16. T. Koschinsky and L. Heinemann, "Sensors for glucose monitoring: technical and clinical aspects," *Diabetes/Metabolism Res Rev* **17**, pp. 113–123, 2001.
17. M. Muller, A. Holmang, O. K. Andersson, H. G. Eichler, and P. Lonnroth, "Measurement of interstitial muscle glucose and lactate concentrations during an oral glucose tolerance test," *Am J Physiology* **271**, pp. E1003–1007, 1996.
18. A. L. Krogstad, P. A. Jansson, P. Gisslen, and P. Lonnroth, "Microdialysis methodology for the measurement of dermal interstitial fluid in humans," *British J Dermatology* **134**, pp. 1005–1012, 1996.
19. U. Hoss, B. Kalatz, R. Gessler, H. J. Pfeleiderer, E. Andreis, M. Rutschmann, H. Rinne, M. Schoemaker, and R. Haug, C Fussgaenger, "A novel method for continuous online glucose monitoring in humans: the comparative microdialysis technique," *Diabetes Technol Ther* **3**, pp. 237–243, 2001.
20. E. M. Janle and P. T. Kissinger, "Microdialysis and ultrafiltration sampling of small molecules and ions from in vivo dialysis fibers," *AACC TDM/Tox* **14**, 1993.
21. S. R. Ash, J. B. Rainer, W. E. Zopp, R. B. Truitt, E. M. Janle, K. P. T, and J. T. Poulos, "A subcutaneous capillary filtrate collector for measurement of blood chemistries," *ASAIO J* **39**, pp. M669–M705, 1993.
22. R. G. Tiessen, W. A. Kaptein, V. K, and J. Korf, "Slow ultrafiltration for continuous in vivo sampling: application for glucose and lactate in man," *Anal Chim Acta* **379**, pp. 327–335, 1999.
23. F. A. M. Baumeister, B. Rolinski, B. R, and P. Emmrich, "Glucose monitoring with long-term subcutaneous microdialysis in neonates," *Pediatrics* **108**, pp. 1187–1192, 2001.
24. R. M. Rhemrev-Boom, R. G. Tiessen, A. A. Jonker, K. Venema, V. P, and J. Korf, "A lightweight measuring device for the continuous in vivo monitoring of glucose by means of ultraslow microdialysis in combination with a miniaturised flow-through biosensor," *Clin Chim Acta* **316**, pp. 1–10, 2002.
25. E. M. Janle and P. T. Kissinger, "Microdialysis and ultrafiltration," *Adv Food Nutr Res* **40**, pp. 183–196, 1996.
26. P. T. Kissinger, "Electrochemical detection in bioanalysis," *J Pharm Biomed Anal* **14**, pp. 871–880, 1996.
27. W. A. Kaptein, J. J. Zwaagstra, V. K, and J. Korf, "Continuous ultraslow microdialysis and ultrafiltration for subcutaneous sampling as demonstrated by glucose and lactate measurements in rats," *Anal Chem* **70**, pp. 4696–4700, 1998.
28. B. L. Carter, E. Shaw, J. T. Olesberg, W. K. Chan, T. C. Hasenberg, and M. E. Flatté, "High detectivity InGaAsSb pin infrared photodetector for blood glucose sensing," **36**(15), pp. 1301–1303, 2000.
29. J. Chen, M. A. Arnold, and G. W. Small, "Comparison of combination and first overtone spectral regions for near infrared calibration models for glucose and other biomolecules in aqueous solutions," *Anal Chem* **76**, pp. 5405–5413, 2004.
30. K. E. Kramer, *Improving the Robustness of Multivariate Calibration Models for the Determination of Glucose by Near-Infrared Spectroscopy*. PhD thesis, University of Iowa, 2005.